


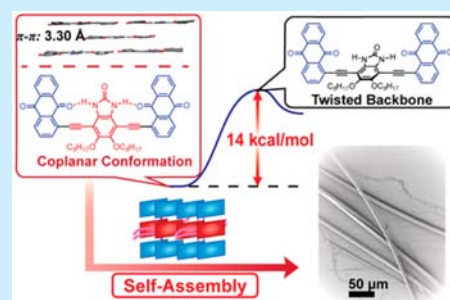
## Molecular Coplanarity and Self-Assembly Promoted by Intramolecular Hydrogen Bonds

Congzhi Zhu, Anthony U. Mu, Yen-Hao Lin, Zi-Hao Guo, Tianyu Yuan, Steven E. Wheeler,<sup>ID</sup> and Lei Fang<sup>\*ID</sup>

Department of Chemistry, Texas A&amp;M University, 3255 TAMU, College Station, Texas 77843, United States

 Supporting Information

**ABSTRACT:** Active conformational control is realized in a conjugated system using intramolecular hydrogen bonds to achieve tailored molecular, supramolecular, and solid-state properties. The hydrogen bonding functionalities are fused to the backbone and precisely preorganized to enforce a fully coplanar conformation of the  $\pi$ -system, leading to short  $\pi$ - $\pi$  stacking distances, controllable molecular self-assembly, and solid-state growth of one-dimensional nano-/microfibers. This investigation demonstrates the efficiency and significance of an intramolecular noncovalent approach in promoting conformational control and self-assembly of organic molecules.



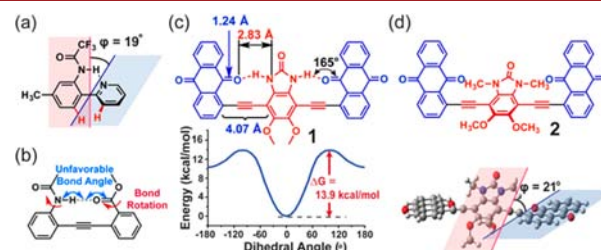
Molecular conformation represents one of the most important structural features for organic molecules. In a  $\pi$ -conjugated compound, the conformation not only shapes the properties of individual molecules but also plays an essential role in determining intermolecular interactions and self-assembly behaviors. Generally, a coplanar backbone of a conjugated molecule facilitates extended  $\pi$ -delocalization,<sup>1</sup> consequently inducing enhanced intramolecular charge transfer and a narrowed band gap.<sup>2</sup> Moreover, coplanarity of conjugated skeletons promotes strong intermolecular  $\pi$ - $\pi$  interactions and electronic coupling,<sup>3</sup> leading to self-assembly in solution,<sup>4</sup> formation of well-defined nano/microstructures,<sup>5</sup> and condensed packing modes in the solid state.<sup>6</sup> Therefore, pursuing coplanar conformations becomes an important strategy in the development of functional  $\pi$ -conjugated organic materials.

The prevailing strategy to achieve such a goal is the construction of fused-ring constitutions by forming additional strands of covalent bonds so that a coplanar conformation is enforced. On one hand, this method is efficient in affording excellent optoelectronic properties of individual molecules<sup>7</sup> and endorses strong intermolecular interactions, which can be further translated into the formation of nano-/microscale assemblies in the solid state.<sup>5b,8</sup> On the other hand, the covalently fused constitution often leads to synthetic and processing challenges and does not allow active control over the torsional conformation of these conjugated molecules.

Alternatively, the employment of intramolecular noncovalent bonds, such as hydrogen bonds,<sup>2a,3,4c,9</sup> B–N Lewis acid–base pairing,<sup>2b,4c,10</sup> metal coordination,<sup>2c</sup> and van der Waals forces,<sup>11</sup> could serve as a promising approach to induce the desired conformation in a  $\pi$ -conjugated molecule while enabling dynamic conformational control. Unlike covalent bonds, the thermodynamically driven formation of noncovalent bonds is reversible,<sup>2a,9b,10a</sup> enabling on-demand control of molecular

conformation and therefore active manipulation over molecular/supramolecular properties.<sup>9b</sup>

Among various types of noncovalent forces, hydrogen bonds stand out as ideal candidates because of their tunable strength and directionality,<sup>12</sup> allowing for precise control of molecular conformation. The introduction of conjugated coplanarity by intramolecular hydrogen bonds, however, is still a challenging task. For example, in a 2-phenylpyridine-based system (Figure 1a), the coplanarity is distorted by 2,2'-H,H repulsion even in the presence of an intramolecular hydrogen bond.<sup>13</sup> Such steric repulsion can be avoided in a 1,2-diphenylethyne derived model compound, in which linear intramolecular hydrogen bonds are installed in parallel (Figure 1b).<sup>2a,9c,d,14</sup> Modern theoretical



**Figure 1.** (a) An intramolecular hydrogen bonded 2-phenylpyridine derivative with a dihedral angle measured from the single crystal structure.<sup>13</sup> (b) A *p*-phenylene ethynylene derivative with a parallel linear hydrogen bond.<sup>16</sup> (c) The structural formula of **1** and the potential energy surface scan [B97D/6-31G(d,p)] of **1** by changing the dihedral angle between the hydrogen bond donating units and accepting units. (d) The structural formula and DFT optimized conformation [B3LYP/6-311G(d,p)] of **2**.

Received: October 27, 2016

Published: November 30, 2016

calculations, however, suggested that the linear hydrogen bond was not as favorable as a bent hydrogen bond in terms of the strength.<sup>15</sup> Moreover, most hydrogen bond donating and accepting moieties were connected to conjugated backbones through rotatable single bonds, which could lead to increased flexibility and hence a greater entropy penalty when adopting the coplanar conformation. In addition, although some promising molecular properties have been reported,<sup>2a,9b</sup> the expected self-assembly and favorable solid-state packing have not been clearly demonstrated yet. Herein, we report the achievement of unambiguous molecular coplanarity, controllable self-assembly, and solid-state fiber formations of a large model  $\pi$ -system **1** (Figure 1c), in which well-defined intramolecular hydrogen bonds play a crucial role in governing these characters.

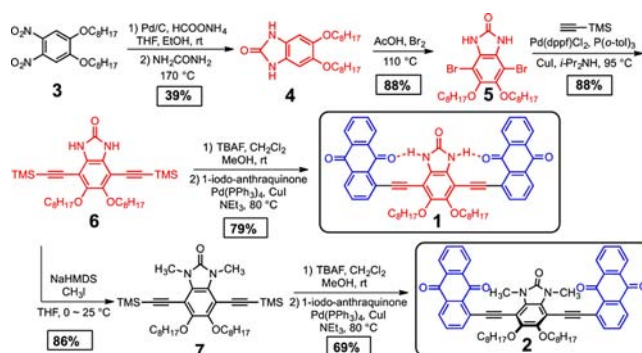
In compound **1**, 1,4-bis(phenylethynyl)benzene was selected as the backbone to avoid the aforementioned 2,2'-H,H steric repulsion.<sup>2a,9c,d,14</sup> The hydrogen bonding moieties were incorporated into the backbone through a fused-ring constitution. This strategy decreases the entropy penalty when the molecule adopts the desired coplanar conformation and, therefore, enhances the strength of the intramolecular hydrogen bonds and the molecular rigidity. Meanwhile, these preorganized hydrogen bonds adopted a bent structure ( $\angle \text{N}\cdots\text{H}\cdots\text{O} \approx 165^\circ$  measured from optimized geometry) and a favorable binding orientation at oxygen.<sup>15,17</sup> Using the reported bond lengths from crystal structures of related building blocks,<sup>18</sup> the distance between hydrogen bonding nitrogen and oxygen was estimated to be  $\sim 2.84$  Å (Figure 1c), falling into the range where hydrogen bonds can be formed effectively.<sup>19</sup> In addition, condensed solid-state packing,<sup>3,6a</sup> aggregation in solution, and self-assembly into well-defined nano/microstructures<sup>5</sup> were expected once the strong hydrogen bonds and high molecular rigidity were achieved.

To validate this molecular design, density functional theory (DFT) was employed to examine the torsional energy landscape of **1**. By fixing the anthraquinone units into the same plane, the torsional potential energy was computed by changing the dihedral angle between the hydrogen bond donor and the anthraquinone plane. The lowest energy was found in the coplanar conformer. The 13.9 kcal/mol potential well suggested that this coplanar conformation was strongly stabilized by the hydrogen bonds (Figure 1c). In parallel, a control molecule (**2**) was designed by inhibiting the hydrogen bonds by methylation. Geometry optimization of this molecule revealed a twisted backbone due to the steric interaction between methyl groups and the anthraquinone units (Figure 1d).

The synthesis toward **1** started with compound **3** prepared according to a literature report (Scheme 1).<sup>20</sup> The linear *n*-octyl chains were installed to increase the solubility of **1** without perturbing the potentially strong  $\pi$ - $\pi$  stacking between the coplanar backbones.<sup>21</sup> After reducing the nitro groups in **3** into amine functionalities, the intermediate was treated directly with molten urea, affording the hydrogen bond donating intermediate (**4**). After bromination, Sonogashira coupling of **5** gave intermediate **6**. The final product **1** was obtained after deprotection of **6** followed by another Sonogashira coupling with 1-iodo-anthraquinone. Compound **2** was prepared from **6** as well. After methylation, the intermediate **7** was converted into **2** using a similar tandem procedure.

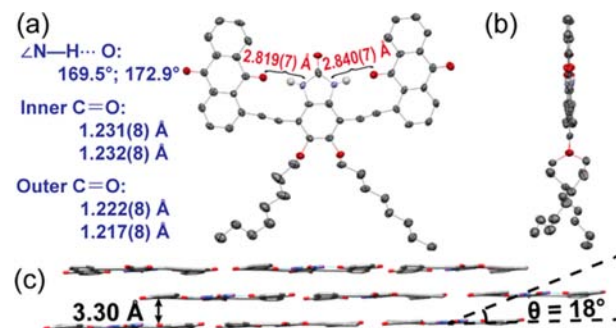
For compound **1**, a remarkable downfield shift of the N–H proton signal (10.15 ppm) was observed in  $\text{CDCl}_3$  at room

### Scheme 1. Synthesis of the Coplanar Model Compound **1** and Its Non-coplanar Counterpart **2**



temperature, in contrast to that in its precursor **6** (7.72 ppm), corroborating the formation of hydrogen bonds in solution at room temperature (Figure S9). Because of the preorganized geometry and rigid nature of the hydrogen bonding moiety, the hydrogen bonds in **1** were expected to be strong and robust in solution and in the solid state. Although variable-temperature  $^1\text{H}$  NMR experiments revealed a slight dissociation of these hydrogen bonds at high temperatures, the chemical shift of the N–H proton remained in the downfield region at 9.99 ppm at  $65^\circ\text{C}$  in  $\text{CDCl}_3$  and 10.27 ppm at  $80^\circ\text{C}$  in  $d_6$ -benzene, respectively (Figure S10). This result indicated that intramolecular hydrogen bonds maintained control over the coplanar molecular conformation even in these boiling solutions. The Fourier transform infrared spectra (Figure S11) showed significantly weakened N–H stretching in **1** ( $3325\text{ cm}^{-1}$ ) compared to a non-hydrogen bonded amide N–H stretching ( $3450$ – $3460\text{ cm}^{-1}$ ),<sup>17</sup> confirming these robust hydrogen bonds in the solid state.

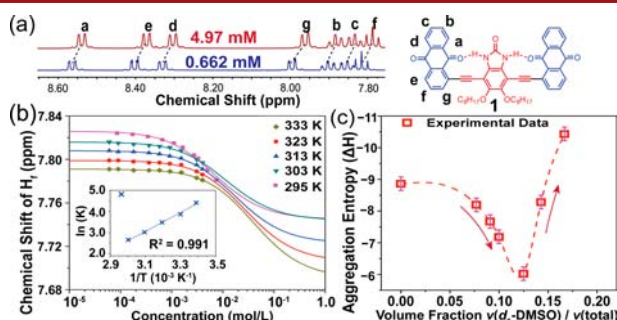
The solid-state structure of **1** was elucidated unambiguously using single crystal X-ray diffraction. The distances between the hydrogen-bond-donating nitrogen atom and the hydrogen-bond-accepting oxygen atom were  $2.819(7)$  Å and  $2.840(7)$  Å on each side respectively (Figure 2a), close to the predicted values, falling into a strong-hydrogen-bond-forming distance.<sup>19</sup> The bond lengths of the inner C=O were longer than those of the outer C=O, in agreement with the decreased carbonyl stretching frequency after accepting hydrogen bonds (Figure S11). An almost coplanar backbone of **1** was observed (dihedral angles less than  $4^\circ$  between the planes of the hydrogen bond donor and acceptors). The ethynylene linker was slightly bent



**Figure 2.** (a) Front view and (b) side view of single crystal structure of **1**. The thermal ellipsoids were scaled to the 50% probability level. (c) A side view of the packing mode of **1** in single crystal. The octyl chains and  $\text{C}_2\text{H}_2\text{Cl}_4$  solvent molecules are omitted for clarity.

in the crystal structure due to the formation of hydrogen bonds. The extended coplanar backbone allows for the condensed packing with a  $\pi$ - $\pi$  stacking distance of 3.30 Å (Figure 2c), which is even shorter than the interlayer distance of graphite (3.35 Å).<sup>22</sup>

In comparison to the control compound **2**, the hydrogen bond formation and the conformational coplanarity of **1** impacted its electronic structure by facilitating a more coherent electronic conjugation of the backbone.<sup>2a,b,9c</sup> Despite the very similar constitutional structures of **1** and **2**, the absorption onset of **1** was 20 nm red-shifted compared to that of **2** (Figure S13). Furthermore, cyclic and differential pulse voltammetry (Figures S15, S16) revealed a lowered LUMO level (−3.44 eV) and a smaller band gap (1.98 eV) of **1** compared to that of **2** (2.04 eV).

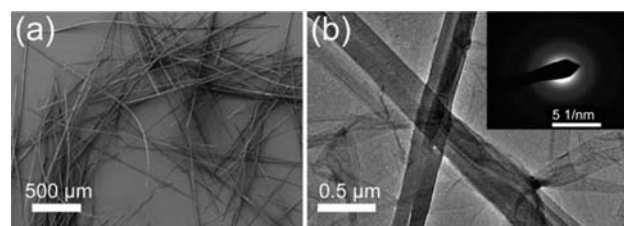


**Figure 3.** (a) The aromatic region of  $^1\text{H}$  NMR spectra of **1** in  $\text{CDCl}_3$  in different concentrations. (b) Temperature- and concentration-dependent  $^1\text{H}$  NMR chemical shifts of proton *f* of **1**, fitted with the isodesmic model; the inset is a van't Hoff plot of aggregation constants at different temperatures. (c) Aggregation enthalpy of **1** in  $\text{CDCl}_3/d_6$ -DMSO mixed solvents while increasing the volume fraction of  $d_6$ -DMSO.

The robust coplanar conformation and tight intermolecular  $\pi$ - $\pi$  stacking of **1** were expected to lead to aggregation/self-assembly of the molecule.<sup>23</sup> To study this character, variable-concentration  $^1\text{H}$  NMR investigations of **1** and **2** were performed in  $\text{CDCl}_3$ . At 295 K, as the concentration of **1** increased, the chemical shifts of the aromatic protons were shifted upfield by  $\sim 20$  ppb (Figure 3a), indicating an aggregation process.<sup>21b,23b</sup> In contrast, the spectra of **2** did not show any significant upfield shift even at a much higher concentration (Figure S17). Such a drastic difference was attributed to the hydrogen bond induced coplanarity of **1**, which enhanced  $\pi$ - $\pi$  stacking in solution and promoted the aggregation, while the twisted backbone and active torsional motion of **2** prevented efficient aggregation. The self-association constant of **1** in  $\text{CDCl}_3$  was calculated to be  $83 \text{ M}^{-1}$  at 295 K, assuming an isodesmic aggregation model. Such a large association constant was comparable with literature reported rigid macrocyclic molecules.<sup>23a</sup> To further quantify the thermodynamic parameters of this aggregation process, self-association constants were measured at different temperatures (Figure 3b). The van't Hoff plot revealed the aggregation enthalpy change of **1** to be  $-8.86 \pm 0.43 \text{ kcal/mol}$  and the entropy change to be  $-21.4 \pm 1.4 \text{ cal/(mol K)}$ , demonstrating a strongly enthalpy-driven process.

To confirm the mechanism of the intramolecular hydrogen bond-promoted self-assembly, the aggregation properties of **1** were investigated with the addition of DMSO, a hydrogen bond competing solvent. In general, the addition of a hydrophilic

solvent, such as DMSO, to a solution of nonpolar compounds is expected to increase the aggregation because of the enhanced hydrophobic interaction in between the solute molecules.<sup>23</sup> For compound **1**, however, it was expected that DMSO should decrease the association constant because of the disruption of intramolecular hydrogen bonds. Indeed, by adding up to 14% (volume fraction) of DMSO to a  $\text{CDCl}_3$  solution of **1**, the aggregation enthalpy became less negative and the association constant decreased (Figure 3c). The hydrophobic aggregation was not observed until the fraction of  $d_6$ -DMSO was increased over 17%, where the hydrophilic nature of DMSO started to predominate. This observation confirmed that the intramolecular hydrogen bond was playing a crucial role to affect the aggregation behavior of **1** by keeping the coplanar conformation and locking the torsional motion. Such controllable aggregation behavior of **1** demonstrated the advantage of the intrinsic dynamic nature of noncovalent bonds when used for conformational control.



**Figure 4.** (a) SEM images of nano-/microfibers of **1** grown from slow evaporation of  $\text{CH}_2\text{Cl}_2$  solutions. (b) TEM images of these fibers with the SAED pattern.

The coplanar backbone, strong anisotropic  $\pi$ - $\pi$  interactions, negative aggregation enthalpy, and the linear peripheral octyl chains distinguished **1** as an ideal candidate for the growth of one-dimensional (1D) organic nano-/microstructures.<sup>21b</sup> From a  $\text{CH}_2\text{Cl}_2$  solution of **1**, 1D fibers with a high aspect ratio (over 500) were obtained feasibly by slow evaporation (Figure 4a) and vapor diffusion (Figure S18). Under scanning electron microscopy (SEM), these fibers showed diameters ranging from 0.3 to  $8 \mu\text{m}$  with the lengths reaching several millimeters (Figure 4a). Under transmission electron microscopy (TEM), a series of ring-like diffraction patterns were observed on selected area electron diffraction (SAED) images (Figure 4b), suggesting a certain extent of ordered arrangements in these fibers, consistent with the powder X-ray diffraction measurement (Figure S20).<sup>24</sup> In contrast, compound **2** did not exhibit any self-assembled fibers due to the lack of the intermolecular aggregation enthalpy as the driving force (Figure S19). Such a distinctive difference between **1** and **2** indicated the significance of using intramolecular noncovalent bonds in promoting the self-assembly of molecules into well-defined solid-state structures.

In conclusion, the investigation of model compound **1** and its non-hydrogen bonded analogue **2** clearly demonstrated the significant impact of preorganized intramolecular hydrogen bonds on molecular conformation and intermolecular self-assembly. These hydrogen bonds were designed to force the molecules to adopt a thermodynamically stable coplanar conformation. This robust coplanarity induced strong intermolecular aggregation and preferential self-assembly into 1D fibers in the solid state. Overall, this work not only establishes a fundamental correlation between intramolecular noncovalent



bonds and molecular/supramolecular properties but also enables practical strategies for tailoring material properties of conjugated organic species through noncovalent conformational control.

## ■ ASSOCIATED CONTENT

### Supporting Information

The Supporting Information is available free of charge on the ACS Publications website at DOI: 10.1021/acs.orglett.6b03225.

Detailed computation data; experimental procedures; characterization data and crystallographic data for **1** (PDF)

Crystallographic data for **1** (CIF)

## ■ AUTHOR INFORMATION

### Corresponding Author

\*E-mail: fang@chem.tamu.edu.

### ORCID

Steven E. Wheeler: 0000-0001-7824-6906

Lei Fang: 0000-0002-2888-5512

### Notes

The authors declare no competing financial interest.

## ■ ACKNOWLEDGMENTS

We thank Texas A&M University (TAMU) for support of this work. We thank Dr. Nattamai Bhuvanesh for X-ray crystallography and diffraction support, Dr. Sarbajit Banerjee for support on electrochemistry. Use of the TAMU Microscopy and Imaging Center, Mr. Rick Littleton, and use of TAMU Materials Characterization Facility are acknowledged. We also thank Dr. Yi Liu at the Molecular Foundry for facility support, who was supported by the Office of Science, Office of Basic Energy Sciences, of the U.S. Department of Energy under Contract No. DE-AC02-05CH11231.

## ■ REFERENCES

- (1) (a) Grozema, F. C.; van Duijnen, P. T.; Berlin, Y. A.; Ratner, M. A.; Siebbeles, L. D. A. *J. Phys. Chem. B* **2002**, *106*, 7791–7795. (b) Levitus, M.; Schmieder, K.; Ricks, H.; Shimizu, K. D.; Bunz, U. H. F.; Garcia-Garibay, M. A. *J. Am. Chem. Soc.* **2001**, *123*, 4259–4265.
- (2) (a) Hu, W.; Zhu, N.; Tang, W.; Zhao, D. *Org. Lett.* **2008**, *10*, 2669–2672. (b) Zhu, C.; Guo, Z.-H.; Mu, A. U.; Liu, Y.; Wheeler, S. E.; Fang, L. *J. Org. Chem.* **2016**, *81*, 4347–4352. (c) Xu, Y.-X.; Zhan, T.-G.; Zhao, X.; Fang, Q.; Jiang, X.-K.; Li, Z.-T. *Chem. Commun.* **2011**, *47*, 1524–1526.
- (3) Lei, T.; Xia, X.; Wang, J.-Y.; Liu, C.-J.; Pei, J. *J. Am. Chem. Soc.* **2014**, *136*, 2135–2141.
- (4) (a) Shu, J.; Dudenko, D.; Esmaili, M.; Park, J. H.; Puniredd, S. R.; Chang, J. Y.; Breiby, D. W.; Pisula, W.; Hansen, M. R. *J. Am. Chem. Soc.* **2013**, *135*, 11075–11086. (b) Wöhrle, T.; Wurzbach, I.; Kirres, J.; Kostidou, A.; Kapernaum, N.; Litterscheidt, J.; Haenle, J. C.; Staffeld, P.; Baro, A.; Giesselmann, F.; Laschat, S. *Chem. Rev.* **2016**, *116*, 1139–1241. (c) van Gorp, J. J.; Vekemans, J. A. J. M.; Meijer, E. W. *J. Am. Chem. Soc.* **2002**, *124*, 14759–14769.
- (5) (a) Chen, S.; Slattum, P.; Wang, C.; Zang, L. *Chem. Rev.* **2015**, *115*, 11967–11998. (b) Zang, L.; Che, Y.; Moore, J. S. *Acc. Chem. Res.* **2008**, *41*, 1596–1608.
- (6) (a) Huang, C.-F.; Wu, S.-L.; Huang, Y.-F.; Chen, Y.-C.; Chang, S.-T.; Wu, T.-Y.; Wu, K.-Y.; Chuang, W.-T.; Wang, C.-L. *Chem. Mater.* **2016**, *28*, 5175–5190. (b) Sutton, C.; Risko, C.; Brédas, J.-L. *Chem. Mater.* **2016**, *28*, 3–16.
- (7) (a) Zhao, W.; Qian, D.; Zhang, S.; Li, S.; Inganäs, O.; Gao, F.; Hou, J. *Adv. Mater.* **2016**, *28*, 4734–4739. (b) Endres, A. H.; Schaffroth, M.; Paulus, F.; Reiss, H.; Wadeh, H.; Rominger, F.; Krämer, R.; Bunz, U. H. F. *J. Am. Chem. Soc.* **2016**, *138*, 1792–1795.
- (8) (a) Balakrishnan, K.; Datar, A.; Oitker, R.; Chen, H.; Zuo, J.; Zang, L. *J. Am. Chem. Soc.* **2005**, *127*, 10496–10497. (b) Luo, J.; Yan, Q.; Zhou, Y.; Li, T.; Zhu, N.; Bai, C.; Cao, Y.; Wang, J.; Pei, J.; Zhao, D. *Chem. Commun.* **2010**, *46*, 5725–5727. (c) Balakrishnan, K.; Datar, A.; Zhang, W.; Yang, X.; Naddo, T.; Huang, J.; Zuo, J.; Yen, M.; Moore, J. S.; Zang, L. *J. Am. Chem. Soc.* **2006**, *128*, 6576–6577. (d) Che, Y.; Datar, A.; Balakrishnan, K.; Zang, L. *J. Am. Chem. Soc.* **2007**, *129*, 7234–7235.
- (9) (a) Qiao, Y.; Guo, Y.; Yu, C.; Zhang, F.; Xu, W.; Liu, Y.; Zhu, D. *J. Am. Chem. Soc.* **2012**, *134*, 4084–4087. (b) Delnoye, D. A. P.; Sijbesma, R. P.; Vekemans, J. A. J. M.; Meijer, E. W. *J. Am. Chem. Soc.* **1996**, *118*, 8717–8718. (c) Hong, J.-H.; Atta, A. K.; Jung, K.-B.; Kim, S.-B.; Heo, J.; Cho, D.-G. *Org. Lett.* **2015**, *17*, 6222–6225. (d) Jones, I. M.; Hamilton, A. D. *Org. Lett.* **2010**, *12*, 3651–3653. (e) Hu, W.; Yan, Q.; Zhao, D. *Chem. - Eur. J.* **2011**, *17*, 7087–7094.
- (10) (a) Wakamiya, A.; Taniguchi, T.; Yamaguchi, S. *Angew. Chem., Int. Ed.* **2006**, *45*, 3170–3173. (b) Wakamiya, A.; Yamaguchi, S. *Bull. Chem. Soc. Jpn.* **2015**, *88*, 1357–1377.
- (11) (a) Guo, X.; Liao, Q.; Manley, E. F.; Wu, Z.; Wang, Y.; Wang, W.; Yang, T.; Shin, Y.-E.; Cheng, X.; Liang, Y.; Chen, L. X.; Baeg, K.-J.; Marks, T. J.; Guo, X. *Chem. Mater.* **2016**, *28*, 2449–2460. (b) Uddin, M. A.; Lee, T. H.; Xu, S.; Park, S. Y.; Kim, T.; Song, S.; Nguyen, T. L.; Ko, S.-j.; Hwang, S.; Kim, J. Y.; Woo, H. Y. *Chem. Mater.* **2015**, *27*, 5997–6007. (c) Jackson, N. E.; Savoie, B. M.; Kohlstedt, K. L.; Olvera de la Cruz, M.; Schatz, G. C.; Chen, L. X.; Ratner, M. A. *J. Am. Chem. Soc.* **2013**, *135*, 10475–10483.
- (12) Bosman, A. W.; Sijbesma, R. P.; Meijer, E. W. *Mater. Today* **2004**, *7*, 34–39.
- (13) Thu, H.-Y.; Yu, W.-Y.; Che, C.-M. *J. Am. Chem. Soc.* **2006**, *128*, 9048–9049.
- (14) (a) Wyrembak, P. N.; Hamilton, A. D. *J. Am. Chem. Soc.* **2009**, *131*, 4566–4567. (b) Miljanic, O. S.; Han, S.; Holmes, D.; Schaller, G. R.; Vollhardt, K. P. C. *Chem. Commun.* **2005**, 2606–2608.
- (15) Morozov, A. V.; Kortemme, T.; Tsemekhan, K.; Baker, D. *Proc. Natl. Acad. Sci. U. S. A.* **2004**, *101*, 6946–6951.
- (16) Cary, J. M.; Moore, J. S. *Org. Lett.* **2002**, *4*, 4663–4666.
- (17) Gellman, S. H.; Dado, G. P.; Liang, G. B.; Adams, B. R. *J. Am. Chem. Soc.* **1991**, *113*, 1164–1173.
- (18) (a) Mavridis, A.; Moustakali-Mavridis, I. *Acta Crystallogr., Sect. B: Struct. Crystallogr. Cryst. Chem.* **1977**, *33*, 3612–3615. (b) Lonsdale, K.; Milledge, J.; El Sayed, K. *Acta Crystallogr.* **1966**, *20*, 1–13.
- (19) Gilli, P.; Pretto, L.; Bertolasi, V.; Gilli, G. *Acc. Chem. Res.* **2009**, *42*, 33–44. N...O distances were used as a measurement of hydrogen bond strength because the hydrogen atoms could not be located precisely according to X-ray diffraction peaks.
- (20) Li, Y.; Chen, Y.; Liu, X.; Wang, Z.; Yang, X.; Tu, Y.; Zhu, X. *Macromolecules* **2011**, *44*, 6370–6381.
- (21) (a) Balakrishnan, K.; Datar, A.; Naddo, T.; Huang, J.; Oitker, R.; Yen, M.; Zhao, J.; Zang, L. *J. Am. Chem. Soc.* **2006**, *128*, 7390–7398. (b) Kastler, M.; Pisula, W.; Wasserfallen, D.; Pakula, T.; Müllen, K. *J. Am. Chem. Soc.* **2005**, *127*, 4286–4296.
- (22) Qie, L.; Chen, W.; Xiong, X.; Hu, C.; Zou, F.; Hu, P.; Huang, Y. *Adv. Sci.* **2015**, *2*, 1500195.
- (23) (a) Zhao, D.; Moore, J. S. *Chem. Commun.* **2003**, *39*, 807–818. (b) Chen, Z.; Lohr, A.; Saha-Möller, C. R.; Würthner, F. *Chem. Soc. Rev.* **2009**, *38*, 564–584. (c) Zhang, C.; Yu, C.; Long, H.; Denman, R. J.; Jin, Y.; Zhang, W. *Chem. - Eur. J.* **2015**, *21*, 16935–16940.
- (24) Luo, J.; Lei, T.; Wang, L.; Ma, Y.; Cao, Y.; Wang, J.; Pei, J. *J. Am. Chem. Soc.* **2009**, *131*, 2076–2077.